

Article

Bipolar Resistive Switching in Hafnium Oxide-Based Nanostructures with and without Nickel Nanoparticles

Markus Otsus ^{*}, Joonas Merisalu , Aivar Tarre , Anna-Liisa Peikolainen , Jekaterina Kozlova, Kaupo Kukli  and Aile Tamm ^{*} 

Institute of Physics, University of Tartu, W. Ostwaldi 1, 50411 Tartu, Estonia

^{*} Correspondence: markus.otsus@ut.ee (M.O.); aile.tamm@ut.ee (A.T.)

Abstract: As research into additives and intentionally introduced impurities in dielectric thin film for enhancing the resistive switching based random access memories (RRAM) continues to gain momentum, the aim of the study was to evaluate the effects of chemically presynthesised Ni nanoparticles (NPs) embedded in a dielectric layer to the overall structure and resistive switching properties. HfO₂-based thin films embedded with Ni NPs were produced by atomic layer deposition (ALD) from tetrakis(ethylmethylamino)hafnium (TEMAH) and the O₂ plasma ALD process onto a TiN/Si substrate. The Ni NPs were separately synthesised through a continuous flow chemistry process and dispersed on the dielectric layer between the two stages of preparing the HfO₂ layer. The nanodevices' morphology and composition were analysed with physical characterisation methods and were found to be uniformly dispersed across the sample, within an amorphous HfO₂ layer deposited around them. When comparing the resistive switching properties of otherwise identical samples with and without Ni NPs, the ILRS/IHRS ratio rose from around a 4 to 9 at 0.2 V reading voltage, the switching voltage dropped from ~2 V to ~1.5 V, and a distinct increase in the endurance characteristics could be seen with the addition of the nanoparticles.

Keywords: atomic layer deposition; hafnium dioxide; resistive switching; transmission electron microscopy; scanning electron microscopy; embedded nanoparticles; nanolaminates



Citation: Otsus, M.; Merisalu, J.; Tarre, A.; Peikolainen, A.-L.; Kozlova, J.; Kukli, K.; Tamm, A. Bipolar Resistive Switching in Hafnium Oxide-Based Nanostructures with and without Nickel Nanoparticles. *Electronics* **2022**, *11*, 2963. <https://doi.org/10.3390/electronics11182963>

Academic Editor: Je-Hyeong Bahk

Received: 25 August 2022

Accepted: 16 September 2022

Published: 19 September 2022

Publisher's Note: MDPI stays neutral with regard to jurisdictional claims in published maps and institutional affiliations.



Copyright: © 2022 by the authors. Licensee MDPI, Basel, Switzerland. This article is an open access article distributed under the terms and conditions of the Creative Commons Attribution (CC BY) license (<https://creativecommons.org/licenses/by/4.0/>).

1. Introduction

Research investigating the resistive switching (RS) phenomena in solid thin films has gained a lot of interest over the last decade, offering the potential for fabricating a new generation of nonvolatile memory devices named resistive random access memories (RRAMs) [1]. Among various thin metal oxide films studied as RS media for memristor cells, HfO₂ films have been mentioned as a media where both unipolar and bipolar RS could be observed depending on the cell design [2–5]. Additionally, hafnium dioxide has a high dielectric constant and exhibits good chemical stability, making it widely studied in RRAM structures [6,7].

Even though many different materials have been extensively studied and evaluated as potential dielectrics for RRAMs, the effects of different additives to or within the dielectric layer have been receiving more and more attention in the last few years to further enhance their properties. It has been proposed that locally controlled impurities within the dielectric layer aid in the formation of conductive filaments (CF). Recent studies have shown the positive effects of doping of the dielectric [8–11] or adding nanodots [6], particles [12], crystals [13], even nanoislands [14] and graphene [15] to the dielectric layer, lowering the SET/RESET voltages of RRAMs, increasing endurance, and helping guide the formation of conductive filaments. Recently, Wang et al. [12] have even proposed the mechanism of a hybrid conductive filament, combining metal and oxygen vacancies-based models, brought about by the addition of a Ag and Cu nanoparticle layer. Introducing controlled impurities has been shown to help modify not only the characteristics relevant to resistive switching

but also the magnetic properties of materials, possibly making way for new applications [16]. For example, we recently showed that layering HfO_2 with Fe_2O_3 allows us to control the magnetic and resistive switching properties of a structure [17]. Nanocomposites of HfO_2 and foreign metal particles have also been studied as RS media [6]. However, the addition of such impurities can also lead to the appearance of different types of RS that can coexist in these structures [18], which may destabilise the RS and complicate programming-reading operations.

There are a number of different ways for depositing HfO_2 when using atomic layer deposition (ALD), but one of the most common ones is $\text{Hf}[\text{N}(\text{CH}_3)(\text{C}_2\text{H}_5)]_4$ (TEMAH). It, alongside other alkylamide-based precursors, is mainly used due to its low deposition temperature and increased nucleation density of HfO_2 . Moreover, for example in comparison to another widely used precursor, HfCl_4 , there is no risk of chlorine residue [15,19]. ALD allows one to deposit conformal nanolayers and effectively coat nanostructures, with a thickness in ideal cases in the Å range, while not being dependent on the size and complexity of the surfaces being coated. ALD is a chemical vapor phase technique, relying on self-limiting reactions controlled by exact purges of reactants and inert gases [20,21]. All of these factors make it an ideal method for building various complex nanodevices.

There have been a number of works looking at different ways of combining HfO_2 and Ni, among them works going over pure Ni [22] and combined metal electrodes [23], as well as embedded Ni nanocrystals [24,25]. Z. Tan et al. showed a clear increase in the memory window of HfO_2 based devices for nonvolatile memory applications after embedding Ni nanocrystals into the dielectric layer. All in all, however, Ni and HfO_2 pairings, be it with Ni as a separate electrode or an additive, remain relatively little researched [26], even though it might provide interesting additional opportunities, for example in relation to Ni magnetic properties. To the best of our knowledge, there have been no previous studies on using presynthesised Ni nanoparticles to be embedded within an ALD HfO_2 dielectric layer. This approach might allow for the use of novel materials, a wider range of synthesis temperatures for both the particles and the nanostructures, as well as reduce the risk of residue from the synthesis of these controlled impurities. Additionally, $\text{HfO}_2 + \text{Ni}$ NPs as a system has not been extensively studied, even though Ni has been shown to enhance resistive switching properties [9].

In the present work, we aim to study how the electrical characteristics of RS and formation mechanisms of CFs in hafnium oxide thin films with and without presynthesised nickel nanoparticles (Figure 1a) differ. Ni nanoparticles (NP) were embedded into a metal insulator metal-like (MIM) nanostructure where the main insulator layer was made using atomic layer deposition (ALD) of hafnium dioxide. The aim of the study was to investigate the physical structure and resistive switching characteristics in otherwise identical samples with and without Ni nanoparticles and show how the addition of Ni NPs affects the nanodevices.

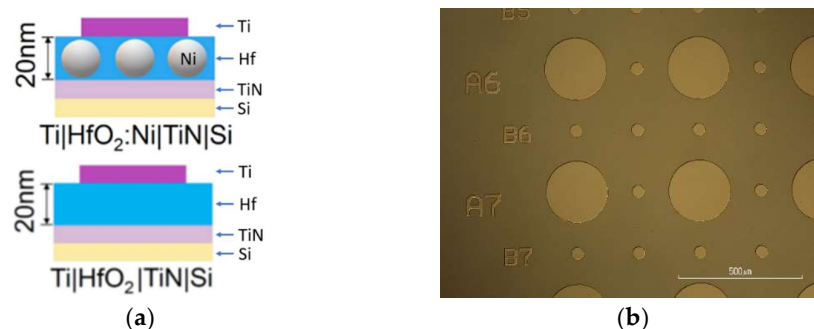


Figure 1. (a) Schematic representation of the nanostructures with and without Ni nanoparticles. (b) Optical microscope top view image of the nanodevices prepared using photolithography.

2. Materials and Methods

The HfO₂ thin films were deposited from Hf[N(CH₃)(C₂H₅)]₄ (TEMAH) and O₂ plasma in a commercial Picosun R-200 Advanced ALD system (Picosun OY, Helsinki, Finland). An initial HfO₂ film was deposited at 220 °C with the first 50 cycles carried out with pulse times 0.3-4-15-4 s (TEMAH-N₂ (purge)-O₂ (plasma)-N₂, respectively). The Ni nanoparticles were dispersed onto the sample by the dip-coating method. For that, the semiprepared wafer was submerged into a solution containing Ni NPs for 90 s, after which a top layer of HfO₂ was deposited on top of the nanoparticles. For the top layer, 8 cycles of only TEMAH were deposited directly onto the particles, with cycle times 0.3-8-0-0 s, followed by 70 full cycles of TEMAH with an O₂ plasma similar to the first 50 cycles. All films were deposited on crystalline TiN-covered substrates cut out of Si(100) wafers with a resistivity of 0.014–0.020 Ω·cm. The Si wafers were boron-doped to concentrations ranging from 5 × 10¹⁸ to 1 × 10¹⁹ cm⁻³. The TiN layer of 10 nm was pregrown by pulsed chemical vapor deposition using a batch TiCl₄/NH₃ process at temperatures of 450–500 °C in an ASM A412 Large Batch 300 mm reactor (Advanced Semiconductor Materials, Almere, The Netherlands) at Fraunhofer IPMS-CNT (Dresden, Germany). Samples without Ni NPs were prepared alongside samples with Ni NPs, effectively having an identical nanolaminate structure with the exception of having been submerged in the solution with dispersed Ni NPs (Figure 1a).

Ni nanoparticles were separately synthesised using a continuous flow synthesis reactor FlowSyn Multi-X™ (Uniqsis, Royston, UK) from nickel(II) 2,4-pentanedionate (Ni(acac)₂, 95%, Alfa Aesar, Haverhill, MA, USA) in continuous mode, using benzyl alcohol as a reducing and particle-stabilising agent. An amount of 30 mM Ni(acac)₂ solution in N,N-dimethylformamide (DMF, reagent grade, Honeywell, Charlotte, NC, USA) was mixed with benzyl alcohol in a volume ratio of 1:1 in flow at 30 °C. The reaction was conducted at 170 °C, with system pressure being 3.5–4 bar and a reaction time of 22 min. The dispersion of Ni particles was collected into a glass vial. The powder was then dried under vacuum, and then redispersed in 2-propanol:benzyl alcohol mixture (1000:1).

The surface morphology was characterised by using a high-resolution scanning electron microscope (SEM) Helios NanoLab 600 (FEI) in a high-resolution mode (10 kV, 86 pA). Compositional analysis was performed using an energy-dispersive X-ray (EDX) spectrometer INCA Energy 350 (Oxford Instruments, Abingdon, UK), attached to the same microscope. Scanning transmission electron microscopy (STEM) and elemental analysis of the nanostructure in cross-sectional orientation were performed in a Cs-corrected Titan Themis 200 microscope (FEI, Hillsboro, OR, USA) equipped with a Super-X EDX system (FEI/Bruker) at 200 kV. EDX maps were acquired using Esprit software version 1.9 (Bruker, Billerica, MA, USA). Thin cross-sectional samples for STEM observations were prepared using the in situ lift-out technique using the Helios Nanolab 600 scanning electron microscope/focused ion beam (FIB) system (FEI, Hillsboro, OR, USA). The same SEM-FIB system was used to carry out initial cross-sectional analysis of the samples.

A diffractometer SmartLab (Rigaku, Tokyo, Japan) with a rotating Cu anode ($\lambda = 0.15406$ nm) working at 8.1 kW was used for X-ray diffraction (XRD) measurements for evaluating the structure of the nanostructures. A small glancing angle of 0.35 degrees was used to reduce the background intensity of the TiN/Si substrate and maximise that of HfO_x thin film.

For the electrical measurements, samples were supplied with titanium top electrodes, prepared by electron-beam evaporator (EBE), and using maskless photolithography (μ MLA Heidelberg Instruments, Zurich, Switzerland). The top electrodes used in the measurements had a diameter of 50 μ m and an area of 0.002 mm² (Figure 1b). Electrical measurements were carried out in a light-proof and electrically shielded box on MPS150 probe station (Cascade Microtech, Beaverton, OR, USA), using a 2636 A source-meter (Keithley Instruments, Cleveland, OH, USA). Endurance measurements, carried out in addition to the characterisation measurements, were done in four sequential source (V) and measure (I)

steps with 0.6 s intervals consisting of SET at 1.5 V, READ at -0.2 V, READ at 0.2 V, and RESET at 1.5 V, respectively, making the time interval between SET and RESET 1.8 s.

3. Results and Discussions

3.1. Initial Characterisation of the Samples

The preliminary size and structure of the particles were found to be relatively uniform, with no large clustering and a polycrystalline structure of Ni. Figure 2a shows a STEM bright field (BF) image of the prepared Ni NPs after synthesis, before being dispersed onto the aimed nanostructure surface. Particles were centrifuged out of the initial solution in order to separate, dry, and disperse the Ni NPs onto a TEM grid. Therefore, the row of particles seen in Figure 2a is not representative of the particle placement on the final device. As can be seen, the as-synthesised Ni NPs had spherical morphology and were polycrystalline. The average NP diameter estimated from STEM images was 81 nm ($\sigma = \pm 3$ nm). Figure 2b shows the overall distribution of the Ni nanoparticles (seen as white dots) after they had been dispersed onto the surface of the initial HfO₂ layer before the deposition of a secondary hafnium layer and the Ti top electrode. As can be seen, the distribution was mainly uniform across the substrate, even though some larger clusters of the NPs were seen. According to the SEM measurements, the average size of the nanoparticles dispersed on the surface was 88 nm, being only slightly larger than the size of the as-synthesised NPs. The average distance between particles was 1.7 μm ($\sigma = \pm 0.1$ μm), and the estimated average density of the Ni NPs was 3 NPs per 10 μm^2 . When comparing the distribution of NPs to those found in previous works [13,24,25], our method of submerging the wafers results in a much sparser distribution, reducing the impact of the particles to the overall surface morphology of the devices. We are also able to say that the NPs are distinctly isolated and separate, so the effect of an individual Ni NP can be expected to be more limited to certain regions of the device and not cover the whole surface. This aspect makes it harder to detect and evaluate their amount and distribution in later stages with various methods, such as XRD, for example, as the concentration of Ni is restricted to discrete locations. However, this also allows us to investigate the effects of separate nanoparticles, not more or less connected webs of particles, or even a distinct layer, which can be assumed to happen in a situation where densely situated metal nanoparticles are prepared through annealing and/or diffuse into the dielectric surrounding it [23,24].

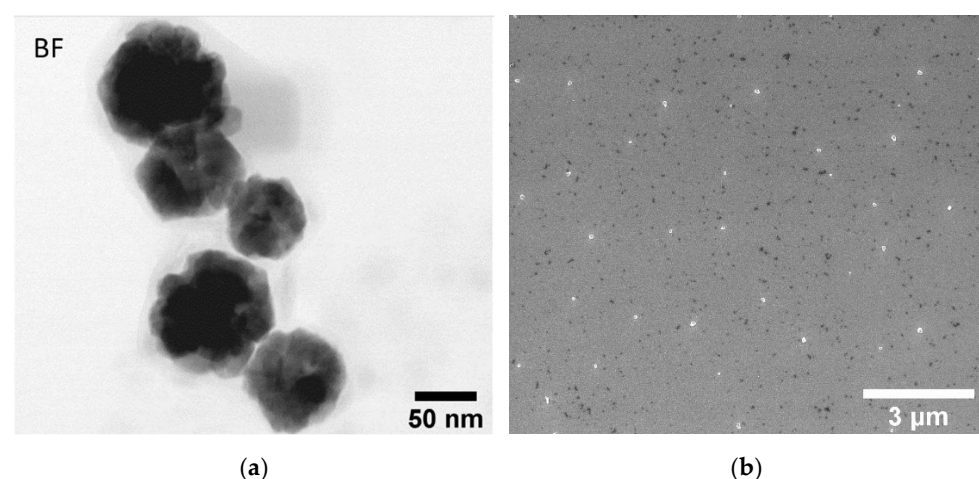


Figure 2. (a) BF STEM image of the as-synthesised Ni NPs measured as a powder. (b) SEM image of Ni NPs dispersed on the substrate before the deposition of the second layer of HfO₂.

The particles were confirmed to be the presynthesised Ni particles by EDX mapping. As can be seen from Figure 3, there is a local increase in nickel concentration in the areas with nanoparticles.

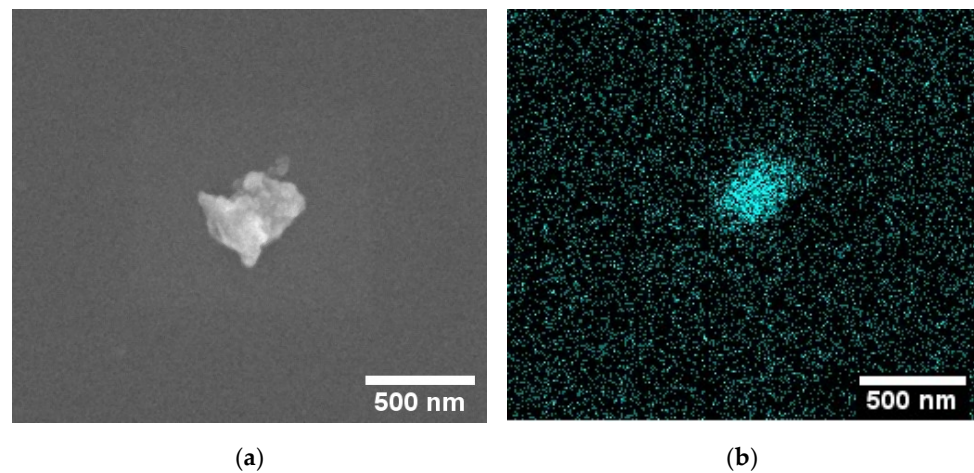


Figure 3. (a) SEM image of Ni nanoparticles on HfO_2/TiN substrate and (b) EDX mapping of Ni of the same region indicating the presumed particles to be, in fact, nickel.

After the ALD of the second HfO_2 layer, Ni NPs became effectively embedded within the structure, and therefore more difficult to locate. Even though larger particles were noticeable from a top-down view, as those seen within the highlighted areas in Figure 4a, the extent to which the Ti top electrode was raised varied significantly, with many particles being very difficult or impossible to see embedded within the structure when examining the electrodes from above. Note, for example, the minimal effect the Ni NP has on the surface of the finished $\text{Ti}/\text{HfO}_2\text{-Ni-HfO}_2/\text{TiN}/\text{Si}$ structure in Figure 4b.

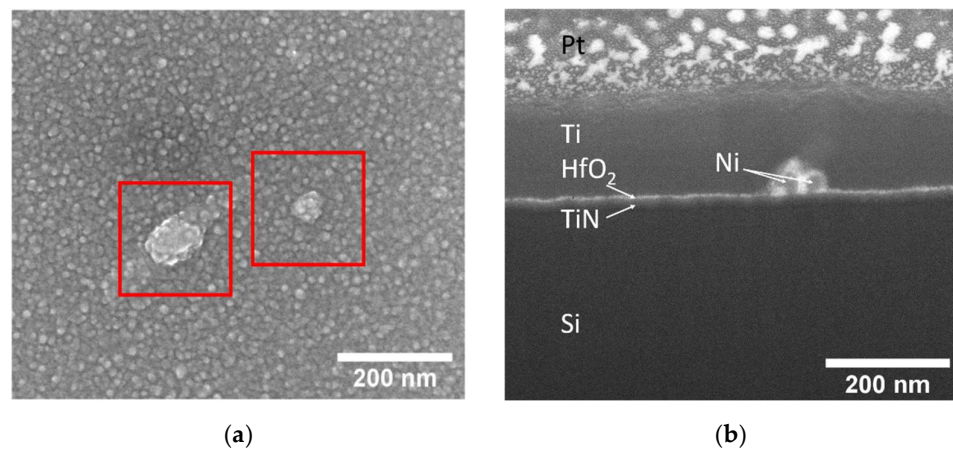


Figure 4. (a) Top-down SEM image of Ni NPs (highlighted) embedded in HfO_2 without the Ti electrode and (b) cross-sectional SEM image of a Ni NP in the finished $\text{Ti}/\text{HfO}_2\text{-Ni-HfO}_2/\text{TiN}/\text{Si}$ nanostructure (Pt on top was deposited to protect the structure from the FIB milling).

Figure 5 depicts XRD patterns of nanostructures with and without Ni nanoparticles measured on a TiN substrate. The measurements indicate an amorphous layer of hafnium oxide in both samples, correlating also with Zhang et al. [27]'s process study of HfO_2 deposited from a similar $\text{TEMAH} + \text{O}_2$ plasma process.

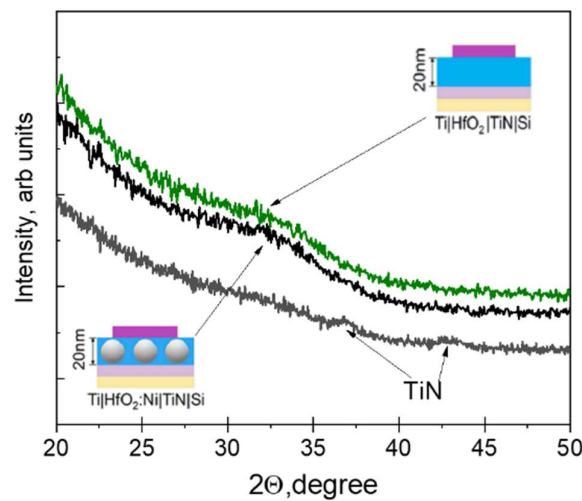


Figure 5. GiXRD patterns from nanostructures with and without Ni nanoparticles and a pure TiN/Si substrate. For the detailed inset color code, see Figure 1a.

Figure 6a presents the results of STEM imaging carried out on a representative Ti/HfO₂/TiN/Si nanostructure. One can see that the constituent HfO₂ films with thicknesses of ~20 nm have formed with defined interfaces between the switching medium and mounting electrodes. The hafnium dioxide layer remains amorphous, as also observed by Zhang et al. [27], whilst the bottom TiN electrode (Figure 6b) and top Ti electrode show a polycrystalline structure.

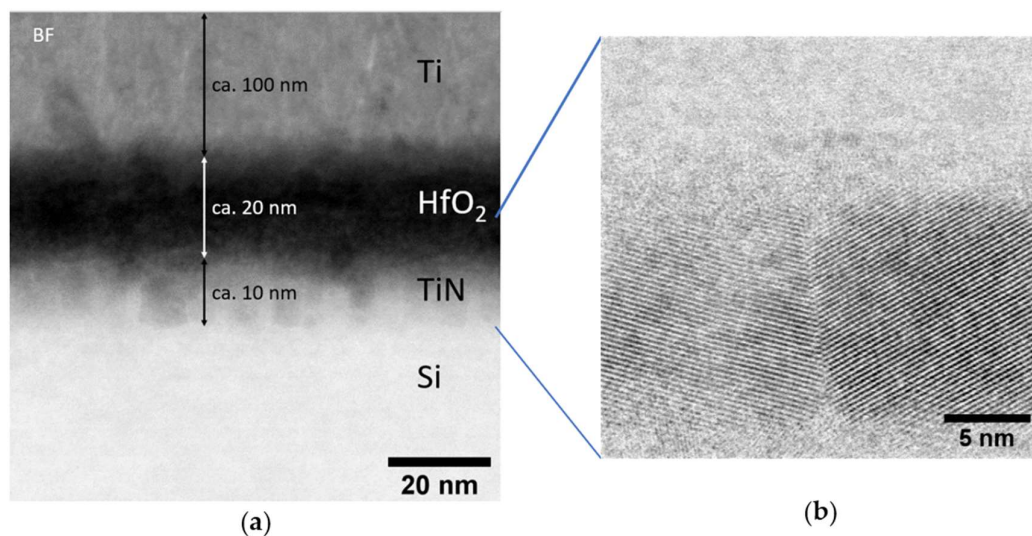


Figure 6. (a) Cross-section of the nanostructure as seen by BF STEM. All layers of the nanostructure are clearly discrete and visible. (b) HfO₂ remains amorphous, while crystal structures are visible in the TiN layer.

A cross-sectional STEM-EDX analysis of the nanostructure with embedded Ni NPs was also performed. The EDX mapping of the region confirmed that we indeed have Ni nanoparticles and could also observe an increased concentration of hafnium and oxygen on the surface of the nanoparticle, suggesting a formation of HfO₂ on top of the Ni NPs. This indicates that the Ni NPs were, in fact, embedded in the dielectric layer and were not merely a part of the top electrode.

All in all, we have shown that we managed to disperse the Ni NPs across the surface with uniformity (Figure 2a) and embed them between a continuous dielectric layer (Figure 4b), thus achieving the goal of creating a basis for the investigation of the effects

of discrete NPs on the appearance of conductive filaments within the nanostructure. It is clear that the preparation of the nanoparticles separately as discrete particles can cause issues such as clustering/agglomeration and also tends to lead to larger particle size, compared to preparing the particles by, for example, annealing a deposited layer within the sample [13,28] or creating nanodots using lithography [6]. It does however allow us to produce our nanodevices at lower temperatures compared to annealing and relieves issues related to lithography.

3.2. Electrical Measurements

The electrically evaluated Ti/HfO₂-Ni-HfO₂/TiN/Si had a MIM-like structure, where commercial highly conductive titanium nitride (TiN) was used as the common bottom electrode and titanium as the top electrode (Figure 1a). Ti/HfO₂-Ni-HfO₂/TiN/Si nanostructure containing several hundred devices as the top electrodes were produced by maskless photolithography as circular dots covering the sample, each dot defining one device (Figure 1b). Several devices per sample were electrically characterised to evaluate the resistive switching performance. RRAMs rely on the initial formation and switching from a high resistive state (HRS) to a low resistive state (LRS) in a so-called SET procedure at a corresponding voltage named the set voltage (U_{SET}). Vice versa, switching the device from LRS to HRS is called a RESET procedure, and the corresponding voltage is denoted as the reset voltage (U_{RESET}). This allows information to be stored in two distinctive resistance states.

The studied nanostructures with and without Ni nanoparticles showed clockwise (CW) bipolar resistive switching (RS) properties (Figures 7 and 8), meaning that the transition from HRS to LRS (SET) takes place at a negative voltage polarity and the RESET at a positive polarity. Some I-V measurements implied the presence of seldom observed counterclockwise (CCW) RS or unipolar RS behaviour. However, it was not possible to achieve a controlled unipolar RS. Supporting the polarity inversion of bipolar RS, G. Vinuesa et al. [29] demonstrated that >13 nm thick HfO₂ thin films exhibit a CW bipolar RS, and less than 8 nm of the same dielectric layer tend to switch in the CCW direction. Based on the latter observation, it could be tempting to assume that the anomalous behaviour could be caused by bipolar RS polarity changes. However, it cannot be unambiguously ruled out that the unipolar RS and the CW RS or the CW and the CCW RS are competing, because the unipolar RS has also been demonstrated earlier by other researchers [30,31].

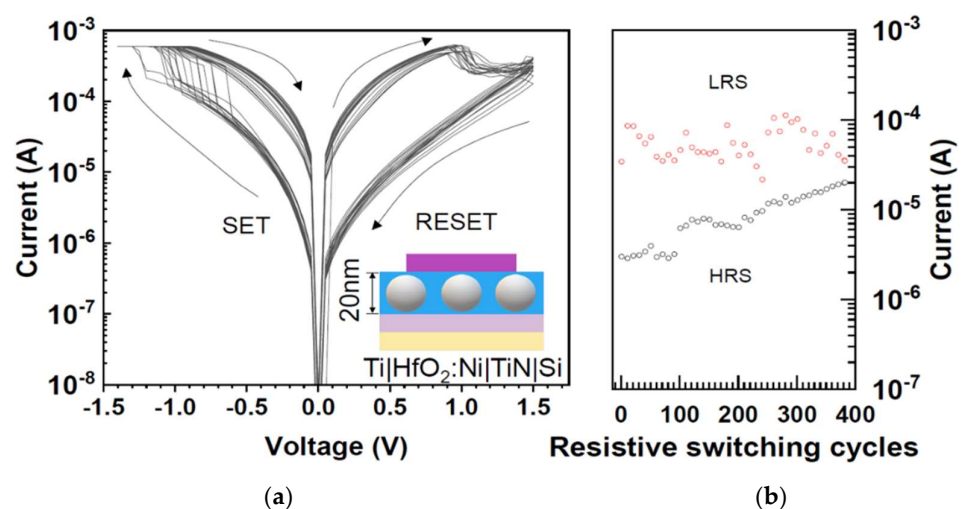


Figure 7. Electrical characterisation of the Ti/HfO₂-Ni-HfO₂/TiN/Si nanostructure with Ni nanoparticles: (a) clockwise I-V curves and (b) endurance measurements at 0.2 V reading voltage. For the detailed inset color code, see Figure 1a.

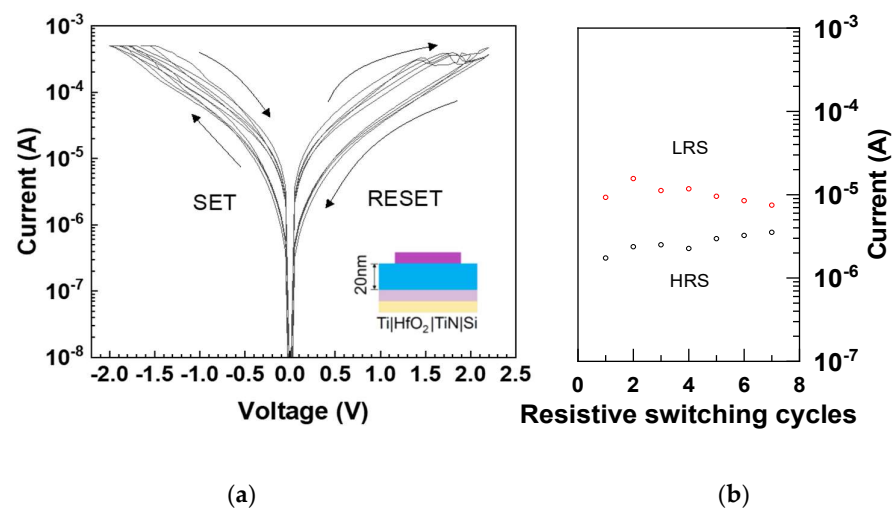


Figure 8. Electrical characterisation of the Ti/HfO₂/TiN/Si nanostructure without Ni nanoparticles: (a) clockwise I-V curves and (b) endurance measurements at 0.2 V reading voltage. For the detailed inset color code, see Figure 1a.

The nanostructures containing Ni nanoparticles tended to demonstrate RS more easily and at lower voltages, i.e., at around 1.5 V compared to the 2 V necessary for the samples without NPs (Figure 7). The device with Ni NPs demonstrated nearly 400 clockwise RS cycles, with set and reset voltages adjusted to -1.5 V and 1.5 V, respectively. Even though in comparison with many other devices, the stability of ours is not outstanding, it is not far off from other works already performed on nanodot based memories [32], and allows us to compare its performance to the samples without NPs. When carefully focusing on the endurance characteristic, one can notice how the memory window gradually diminishes and as can be seen in the figures, the switching voltages demonstrate a difference between LRS and HRS over slightly more than one order of magnitude with an average I_{LRS}/I_{HRS} ratio of around 9 at 0.2 V reading voltage.

It must be pointed out that 400 RS cycles is not yet significant from a device engineering point of view. Nevertheless, when compared to the performance of the sample without Ni NPs, the behaviour of the latter device remained inferior, even though the nanostructures were prepared during the same HfO₂ deposition process. Figure 8 demonstrates that the nanostructures without nanoparticles have a memory window smaller than one order of magnitude, with an average I_{LRS}/I_{HRS} ratio of around 4 at a 0.2 V reading voltage. With a rapid deterioration of the memory window, only a scarce endurance performance could be measured (Figure 8).

Discussing the underlying RS mechanisms remains somewhat speculative, as studying the CF with direct methods like HRTEM was unsuccessful in our current study, which is not surprising, as it is known to be a challenging objective [33]. The Ni NPs are a source of an electrochemically active metal, supporting RS mechanisms like thermochemical metallisation, dominating in unipolar RS, and electrochemical metallisation mechanism (ECM), where ionic migration of active metal ions causes forming and disruption of metallic filaments by changing the direction of the electric field [31,33,34]. In addition to ECM, oxygen deficiency, i.e., the existence of oxygen vacancies can play a key role in the formation of CFs. In the current study, the top electrode of Ti can have the role of an oxygen scavenger aiding to provide oxygen vacancies in the main host media of hafnia. Y. Zhang et al. [35] have demonstrated that, in structures with symmetric inert electrodes, for example, Pt/HfO₂/Pt and also in asymmetric Ti/HfO₂/Pt structures, the valence change mechanism (VCM), in addition to Joule heating, is of paramount importance in the formation mechanism of CFs. VCM is based on the migration of oxygen vacancies, with the temperature-aided formation of CFs, consisting of conductive phases with a changed valence state in host media, relying on redox electrochemistry [16,35]. From another perspective, S. Wang et al. [12] offer a third

possibility of hybrid CFs consisting of two intrinsic regions—one formed by the migration of oxygen vacancies (VCM) and another region formed by metallic ions (ECM). Explaining the rather low endurance performance for the devices with Ni NPs, J. Munoz-Goriz et al. [36] demonstrated the degradation of unipolar RS in Ni/HfO₂/n+-Si devices owing to the diffusion of Ni into the host media, gradually increasing SET currents due to the strengthening CF and cascading the degradation.

The study demonstrated that, even though the samples without NPs already showed clockwise bipolar resistive switching, adding the Ni nanoparticles to the HfO₂ RS medium lowered the switching voltages and enhanced the overall RS performance.

4. Conclusions

In this study, the effect of Ni NPs embedded in a 20 nm thick dielectric HfO₂ film was investigated. The particles were found to be uniformly distributed across the surface and embedded in a discrete continuous layer of amorphous HfO₂ thin film. A clear distinction between resistive switching properties of nanostructures with and without the addition of Ni NPs to the hafnium dioxide dielectric layer was made. The study demonstrated that all samples could show both clockwise and counterclockwise bipolar resistive switching. Adding Ni nanoparticles to the HfO₂ RS medium lowered switching voltages from ~2 V to ~1.5 V, with an I_{LRS}/I_{HRS} ratio of 9, and enhanced the overall RS performance. The MIM-like stack structured as Ti/HfO₂-Ni-HfO₂/TiN/Si was able to carry out approximately 400 bipolar switching cycles before degradation. At the same time, even though the nanostructure without Ni NPs also exhibited a distinct memory window with an I_{LRS}/I_{HRS} ratio of 4, it remained markedly smaller and only unstable endurance measurements were realised. The present study provided valuable information and possible inspiration for further investigations, as further studies should evidently comprise investigations of the effect of the average size and density of metallic nanodots as well as the influence of the thickness and processing temperature of the host medium layer.

Author Contributions: Conceptualisation, A.T. (Aile Tamm) and M.O.; formal analysis, A.T. (Aivar Tarre) and J.M.; investigation, M.O., J.M., J.K., and A.-L.P.; resources, A.T. (Aile Tamm) and K.K.; writing—original draft preparation, M.O., J.M., J.K., A.T. (Aile Tamm), A.-L.P., K.K., and A.T. (Aivar Tarre); funding acquisition, K.K. and A.T. (Aile Tamm). All authors have read and agreed to the published version of the manuscript.

Funding: The work was partially supported by the European Regional Development Fund Projects “Emerging Orders in Quantum and Nanomaterials” (TK134) and Estonian Research Agency (PRG753 and PRG4).

Data Availability Statement: Data is contained within the article.

Acknowledgments: Tauno Kahro is thanked for his assistance in using photolithography and Aarne Kasikov is thanked for his assistance in using EBE. The authors are indebted to the European Regional Development Fund Project “Centre of Nanomaterials Technologies and Research” (NAMUR+, Project No. 2014–2020.4.01.16-0123).

Conflicts of Interest: The authors declare no conflict of interest.

References

1. Lanza, M.; Wong, H.-S.P.; Pop, E.; Ielmini, D.; Strukov, D.; Regan, B.C.; Larcher, L.; Villena, M.A.; Yang, J.J.; Goux, L.; et al. Recommended Methods to Study Resistive Switching Devices. *Adv. Electron. Mater.* **2019**, *5*, 1800143. [[CrossRef](#)]
2. Pedretti, G.; Ielmini, D. In-Memory Computing with Resistive Memory Circuits: Status and Outlook. *Electronics* **2021**, *10*, 1063. [[CrossRef](#)]
3. Lim, E.W.; Ismail, R. Conduction Mechanism of Valence Change Resistive Switching Memory: A Survey. *Electronics* **2015**, *4*, 586–613. [[CrossRef](#)]
4. Chen, A. A review of emerging non-volatile memory (NVM) technologies and applications. *Solid-State Electron.* **2016**, *125*, 25–38. [[CrossRef](#)]

5. Zahoor, F.; Zulkifli, T.Z.A.; Khanday, F.A. Resistive Random Access Memory (RRAM): An Overview of Materials, Switching Mechanism, Performance, Multilevel Cell (mlc) Storage, Modeling, and Applications. *Nanoscale Res. Lett.* **2020**, *15*, 1–26. [[CrossRef](#)]
6. Li, Y.; Tang, J.; Gao, B.; Sun, W.; Hua, Q.; Zhang, W.; Li, X.; Zhang, W.; Qian, H.; Wu, H. High-Uniformity Threshold Switching HfO₂-Based Selectors with Patterned Ag Nanodots. *Adv. Sci.* **2020**, *7*, 2002251. [[CrossRef](#)]
7. Tomer, S.; Vandana; Panigrahi, J.; Srivastava, R.; Rauthan, C. Importance of precursor delivery mechanism for Tetra-kis-ethylmethylaminohafnium/water atomic layer deposition process. *Thin Solid Film.* **2019**, *692*, 137629. [[CrossRef](#)]
8. Qin, Y.; Wang, Z.; Ling, Y.; Cai, Y.; Huang, R. A TaO_x-Based RRAM with Improved Uniformity and Excellent Analog Characteristics by Local Dopant Engineering. *Electronics* **2021**, *10*, 2451. [[CrossRef](#)]
9. Yan, L.; Ruan, L.; Luo, F.; Tong, J.; Sun, C.; Zheng, Y.; Han, X.; Zhang, Y.; Zhang, X. Enhanced resistive switching behavior of CH₃NH₃PbI₃ based resistive random access memory by nickel doping. *Vacuum* **2022**, *198*, 110862. [[CrossRef](#)]
10. Guo, T.; Huang, H.; Huang, X.; Wang, Y.; Duan, L.; Xu, Z. Modulation of resistive switching and magnetism of HfOx film by Co doping. *J. Alloy. Compd.* **2022**, *921*, 166248. [[CrossRef](#)]
11. Han, G.; Chen, Y.; Liu, H.; Wang, D.; Qiao, R. Impacts of LaOx Doping on the Performance of ITO/Al₂O₃/ITO Transparent RRAM Devices. *Electronics* **2021**, *10*, 272. [[CrossRef](#)]
12. Wang, S.; Ning, X.; Hao, A.; Chen, R. Metal nanoparticles layer boosted resistive switching property in NiFe₂O₄-based memory devices. *J. Alloy. Compd.* **2022**, *908*, 164569. [[CrossRef](#)]
13. Yeh, P.; Chen, L.; Liu, P.; Wang, D.; Chang, T. Metal nanocrystals as charge storage nodes for nonvolatile memory devices. *Electrochimica Acta* **2007**, *52*, 2920–2926. [[CrossRef](#)]
14. Wang, J.; Li, L.; Huan, H.; Pan, X.; Nonnenmann, S.S. Highly Uniform Resistive Switching in HfO₂ Films Embedded with Ordered Metal Nanoisland Arrays. *Adv. Funct. Mater.* **2019**, *29*, 1808430. [[CrossRef](#)]
15. Kahro, T.; Tarre, A.; Käämbre, T.; Piirsoo, H.-M.; Kozlova, J.; Ritslaid, P.; Kasikov, A.; Jõgiaas, T.; Vinuesa, G.; Dueñas, S.; et al. Hafnium Oxide/Graphene/Hafnium Oxide-Stacked Nanostructures as Resistive Switching Media. *ACS Appl. Nano Mater.* **2021**, *4*, 5152–5163. [[CrossRef](#)]
16. Müller, C.; Deleruyelle, D.; Ginez, O.; Portal, J.-M.; Bocquet, M. Design challenges for prototypical and emerging memory concepts relying on resistance switching. In Proceedings of the 2011 IEEE Custom Integrated Circuits Conference (CICC), San Jose, CA, USA, 19–21 September 2011. [[CrossRef](#)]
17. Kalam, K.; Otsus, M.; Kozlova, J.; Tarre, A.; Kasikov, A.; Rammula, R.; Link, J.; Stern, R.; Vinuesa, G.; Lendínez, J.M.; et al. Memory Effects in Nanolaminates of Hafnium and Iron Oxide Films Structured by Atomic Layer Deposition. *Nanomaterials* **2022**, *12*, 2593. [[CrossRef](#)] [[PubMed](#)]
18. Chung, Y.-L.; Cheng, W.-H.; Jeng, J.-S.; Chen, W.-C.; Jhan, S.-A.; Chen, J.-S. Joint contributions of Ag ions and oxygen vacancies to conducting filament evolution of Ag/TaO_x/Pt memory device. *J. Appl. Phys.* **2014**, *116*, 164502. [[CrossRef](#)]
19. Kamiyama, S.; Miura, T.; Nara, Y.; Arikado, T. Atomic Layer Deposition of Hafnium Silicate Gate Dielectric Films Using Hf[N(CH₃)(C₂H₅)₄] and SiH[N(CH₃)₂]₃ Precursors. *Electrochem. Solid-State Lett.* **2005**, *8*, G215. [[CrossRef](#)]
20. Johnson, R.W.; Hultqvist, A.; Bent, S.F. A brief review of atomic layer deposition: From fundamentals to applications. *Mater. Today* **2014**, *17*, 236–246. [[CrossRef](#)]
21. Leskelä, M.; Ritala, M. Atomic Layer Deposition Chemistry: Recent Developments and Future Challenges. *Angew. Chem. Int. Ed.* **2003**, *42*, 5548–5554. [[CrossRef](#)]
22. Gonzalez, M.B.; Acero, M.C.; Beldarrain, O.; Zabala, M.; Campabadal, F. Investigation of the resistive switching behavior in Ni/HfO₂-based RRAM devices. In Proceedings of the 2015 10th Spanish Conference on Electron Devices (CDE), Aranjuez, Spain, 11–13 February 2015. [[CrossRef](#)]
23. Chen, Y.Y.; Pourtois, G.; Wang, X.P.; Adelman, C.; Goux, L.; Govoreanu, B.; Pantisano, L.; Kubicek, S.; Altissime, L.; Jurczak, M.; et al. Switching by Ni Filaments in a HfO₂ Matrix: A New Pathway to Improved Unipolar Switching RRAM. In Proceedings of the 2011 3rd IEEE International Memory Workshop (IMW), Monterey, CA, USA, 22–25 May 2011. [[CrossRef](#)]
24. Tan, Z.; Samanta, S.K.; Yoo, W.J.; Lee, S. Self-assembly of Ni nanocrystals on HfO₂ and N-assisted Ni confinement for nonvolatile memory application. *Appl. Phys. Lett.* **2005**, *86*, 013107. [[CrossRef](#)]
25. Yang, F.M.; Chang, T.C.; Liu, P.-T.; Chen, U.S.; Yeh, P.H.; Yu, Y.C.; Lin, J.Y.; Sze, S.M.; Lou, J.C. Nickel nanocrystals with HfO₂ blocking oxide for nonvolatile memory application. *Appl. Phys. Lett.* **2007**, *90*, 222104. [[CrossRef](#)]
26. Napolean, A.; Sivamangai, N.M.; Rajesh, S.; NaveenKumar, N.; Nithya, N.; Kamalnath, S.; Aswathy, N. Review on role of nanoscale HfO₂ switching material in resistive random access memory device. *Emergent Mater.* **2022**, *5*, 489–508. [[CrossRef](#)]
27. Zhang, X.-Y.; Hsu, C.-H.; Cho, Y.-S.; Zhang, S.; Lien, S.-Y.; Zhu, W.-Z.; Xiong, F.-B. Rapid thermal processing of hafnium dioxide thin films by remote plasma atomic layer deposition as high-k dielectrics. *Thin Solid Film.* **2018**, *660*, 797–801. [[CrossRef](#)]
28. Liu, C.-Y.; Huang, J.-J.; Lai, C.-H. Resistive switching characteristics of a Pt nanoparticle-embedded SiO₂-based memory. *Thin Solid Film.* **2012**, *529*, 107–110. [[CrossRef](#)]
29. Vinuesa, G.; García, H.; González, M.B.; Kalam, K.; Zabala, M.; Tarre, A.; Kukli, K.; Tamm, A.; Campabadal, F.; Jiménez, J.; et al. Effect of Dielectric Thickness on Resistive Switching Polarity in TiN/Ti/HfO₂/Pt Stacks. *Electronics* **2022**, *11*, 479. [[CrossRef](#)]
30. González-Cordero, G.; González, M.; Zabala, M.; Kalam, K.; Tamm, A.; Jiménez-Molinos, F.; Campabadal, F.; Roldán, J. Study of RTN signals in resistive switching devices based on neural networks. *Solid-State Electron.* **2021**, *183*, 108034. [[CrossRef](#)]

31. Muñoz-Gorriz, J.; Miranda, E.; Suñé, J.; Acero, M.C.; Gonzalez, M.B.; Campabadal, F. Microelectronic Devices and Technologies. In Proceedings of the 1st International Conference on Microelectronic Devices and Technologies (MicDAT'2018), Barcelona, Spain, 20–22 June 2018.
32. Banerjee, W.; Liu, Q.; Hwang, H. Engineering of defects in resistive random access memory devices. *J. Appl. Phys.* **2020**, *127*, 051101. [[CrossRef](#)]
33. Petzold, S.; Zintler, A.; Eilhardt, R.; Piros, E.; Kaiser, N.; Sharath, S.U.; Vogel, T.; Major, M.; McKenna, K.P.; Molina-Luna, L.; et al. Forming-Free Grain Boundary Engineered Hafnium Oxide Resistive Random Access Memory Devices. *Adv. Electron. Mater.* **2019**, *5*, 1900484. [[CrossRef](#)]
34. Kärkkäinen, I. *Resistive Switching in ZrO₂ Based Metal-Oxide-Metal Structures*; Forschungszentrum Jülich: Jülich, Germany, 2014.
35. Zhang, Y.; Mao, G.-Q.; Zhao, X.; Li, Y.; Zhang, M.; Wu, Z.; Wu, W.; Sun, H.; Guo, Y.; Wang, L.; et al. Evolution of the conductive filament system in HfO₂-based memristors observed by direct atomic-scale imaging. *Nat. Commun.* **2021**, *12*, 1–10. [[CrossRef](#)]
36. Muñoz-Gorriz, J.; González, M.; Miranda, E.; Suñé, J.; Campabadal, F. Impact of the forming and cycling processes on the electrical and physical degradation characteristics of HfO₂-based resistive switching devices. *Thin Solid Film.* **2020**, *706*, 138027. [[CrossRef](#)]